Mohr–Coulomb characterisation of inorganically-bound core materials

Philipp Lechner [a,*], Jens Stahl [a], Christoph Hartmann [a], Florian Ettemeyer [b], Wolfram Volk [a]

[a] Chair of Metal Forming and Casting, Technical University of Munich, Walther-Meissner-Strasse 4, 85748 Garching, Germany
[b] Fraunhofer Research Institution for Casting, Composite and Processing Technology IGCV, Zeppelinstrasse 15, 85748 Garching, Germany

1. Introduction

Foundry cores are used in the casting industry to shape contours in the cast part, which cannot be generated by the mould alone, according to Bührig-Polaczek and Träger (2010). Polzin (2014) describes the constituents of core materials. They consist of sand and a binding agent which is holding the individual grains together. The core is placed into the mould before the casting and destroyed afterwards, which is called de-coring, as stated by Stauder et al. (2018). Kammerer and Essbauer (2009) state that inorganically-bound (IOB) foundry core materials are important in modern mass production, since they are used in several high-volume casting techniques especially in the automotive industry. Pabel et al. (2012) claim that they influence the quality of the casting product to a high degree, due to the central role they play in the mould during the casting process.

1.1. Mechanical modelling of core materials

Despite this technical and economic importance of sand cores, we have no consistent mechanical material model to accurately describe the behaviour of this material. Compared to other engineering materials, the knowledge of foundry core materials is limited. Galles and Beckermann (2015) proposed to model the failure of foundry cores with a Drucker–Prager yield criterion. Thorborg et al. (2020) utilised a Drucker–Prager model for core materials, as well. Stauder et al. (2019) modelled it with a Mohr–Coulomb criterion, while Dong et al. (2010) proposed a maximum principle stress criterion. Caylak and Mahnken (2010) showed that the strength of sand cores is significantly influenced by the hydrostatic stress in the material, which coincides with analogies to geological materials and is not compatible with a maximum principle stress criterion, since this criterion neglects the influence of the hydrostatic stress on the material strength.

However, no published work fully validated the proposed material models. They are based on analogies to materials, which have a similar morphological structure. Today's dimensioning process of sand cores is mostly based on experience. The goal of this article is to create a consistent and validated finite element material model, which allows production processes like core handling to be simulated.

In a series of previous articles, Lechner et al., showed that inorganically-bound foundry cores follow a combination of weakest-link theory (Lechner et al., 2018) and the Mohr–Coulomb yield criterion (Lechner et al., 2021).

1.2. Influence of binder amount and storage time on the mechanical behaviour

There is research on the influence of the binder amount on the mechanical strength. Stachowicz et al. (2011) studied the influence of the binder amount on the strength of microwaved-hardened inorganic core materials. Furthermore, they analysed the influence of core shooting

* Corresponding author.
E-mail address: philipp.lechner@utg.de (P. Lechner).

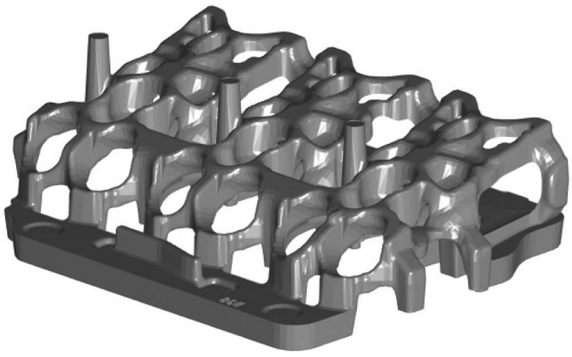

Fig. 1. Three cylinder water jacket core used for validation experiments in this article.

parameters on the mechanical properties of sodium silicate olivine moulding sands (Stachowicz et al., 2020). Vasková et al. (2020) studied the influence of alkali silicate-based inorganic binders and several sands on the mechanical properties of the resulting cores. Granat et al. (2008) varied the binder amount between 0.5% and 5.0% and determined the bending and the compressive strength. Banganayi et al. (2020) studied the influence of the binder amount, the hardening time and the hardening temperature for a novel inorganic binder system. The influence of the storage time on the core strength has been studied as well: Fan et al. (2004) have analysed the influence of the storage time on the core strength. Furthermore, Stauder et al. (2016) have determined the influence of the storage time on the mechanical properties of several organic sand-binder systems, including the material strength and the Young's modulus. Xin et al. (2020) determined the tensile strength for inorganic core materials immediately after the production and after a 24 h storage period and analysed the influence of several additives.

However, there is no work on the influence of the binder amount and the storage time on the Poisson ratio. Furthermore, the existing research does not provide the influence of these production parameters on a complete material model (elastic model and yield criterion), which can be implemented in FEM.

1.3. Research goal

In this article, the influence of the binder amount and the storage time after the core shooting on the mechanical parameters of IOB materials will be studied. The goal is to show how typical manufacturing conditions along the core's life-cycle affect the parameters of the failure model. The dimensioning process of the cores has to consider handling processes from the core shooting machine to the mould. The core strength can be adapted by the binder amount used, but the influence on the Mohr–Coulomb parameters and the elastic properties is still unknown. To determine the optimal binder amount for a specific core, these handling processes have to be simulated to acquire the minimal strength necessary. This article will provide the methodology to predict the parameters of a Mohr–Coulomb yield criterion for specific process conditions and to quantify the binder amount based on this necessary strength with a data-based model (e.g. regression). The binder amount, the storage time and the temperature of the specimens will be varied to study their influence on the material parameters. Furthermore, the material model will be applied to a complex water jacket core geometry and the failure will be predicted under different load cases in order to show that these methods are applicable to highly complex foundry cores.

2. Materials and methods

2.1. Specimens

The specimens utilised for this article, are a three-cylinder water jacket core, which is shown in Fig. 1 and a bending beam with the dimensions 173.5 mm × 22.8 mm × 22.8 mm. This beam was used for the material characterisation. The three point bending experiments were done with the specimen at its full length. The compression test was performed on cubes with the dimensions 20 mm × 22.8 mm × 22.8 mm, which were acquired by shortening the original beams.

Consistent with previous studies of Lechner et al. (2020), the specimens were produced on a Loramendi core shooting machine SLC2 25L (Loramendi S.Coop., Vitoria, Spain) with a heated core box and a hot-gas drying device. An inorganic Inotec binder system (ASK Chemicals GmbH, Hilden Germany) was utilised to bind a H32 silica sand (Quarzwerke GmbH, Frechen, Germany). This system is based on sodium silicate and consists of a liquid component EP 4158 and a powder additive TC 4500. The tool temperature was 155 °C and the air temperature was set to 170 °C. The cores were hardened in the heated tool for 30 s, which induces a condensation reaction in the binder system and builds the binder bridges between the individual sand grains. Holtzer and Kmita (2020) describe the chemical reactions necessary for the hardening of sodium silicate binder systems in detail. Three amounts of binders were used: 1.5%, 2% and 2.5% of liquid binder with their respective amounts of additive (1.2%, 1.6% and 2%). The binder masses are measured relative to the sand mass in wt%. These parameters are chosen such, that they resemble typical industrial production parameters to enhance the applicability of the results for industrial core production. The storage time is varied between 10 s and 24 h since these storage times represent the lower and upper boundaries, which are of interest for material modelling. The cores are handled for the first time directly after the core shooting. The condensation reaction continues after the core is removed from the tool. Therefore, the mechanical properties are characterised again after 24 h. Furthermore, one set of

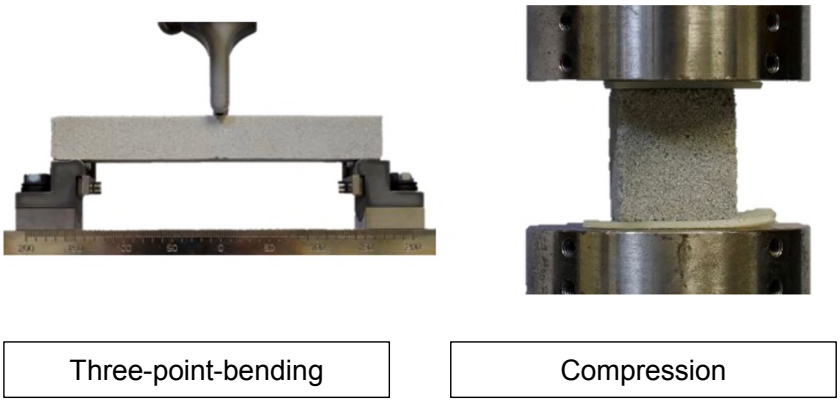

Fig. 2. Experimental setup for the three-point-bending (left) and the compression (right) experiments.

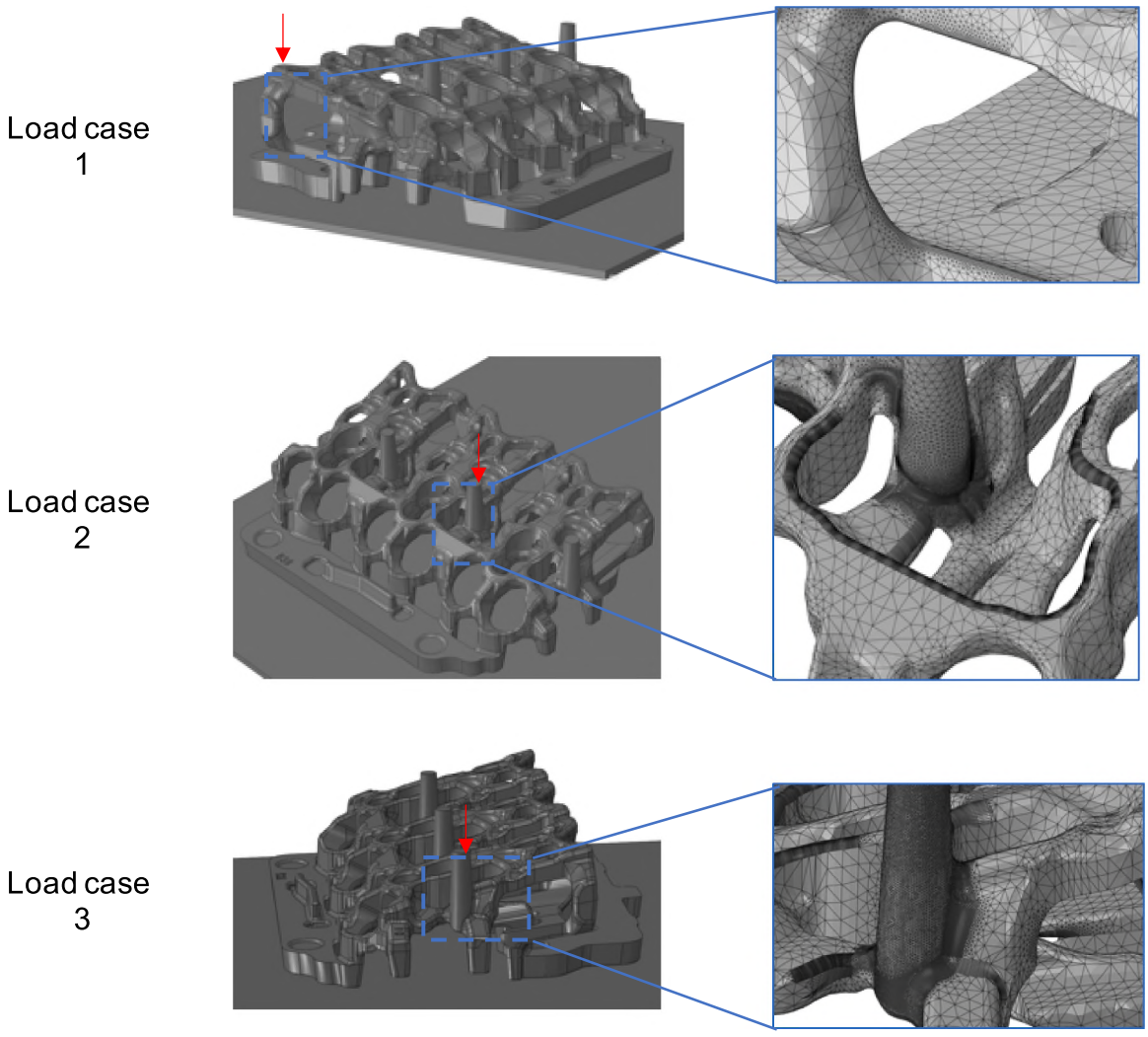

Fig. 3. Load cases of the water jacket core. The core is standing on a plate and is subjected to a vertical force by the testing machine. The load point is indicated by the red arrow. The mesh of the regions of interest is shown on the right side. In the area of increased stresses the mesh is refined.

specimens is heated to 450 °C for 30 min to emulate the casting with aluminium. Bargaoui et al. (2017) showed similar temperatures in the core for an aluminium casting process.

2.2. Material characterisation

The methodology follows previous publications of Lechner et al. for the material characterisation. In a first step, the Young's modulus E and the shear modulus G are determined via impulse excitation technique. Assuming isotropic behaviour, the Poisson ratio ν can be calculated with (EN, 2006):

$$\nu = \frac{E}{2G} - 1 \tag{1}$$

The specific test bench is described by Lechner et al. (2020). In a second step, the material parameters for a Mohr–Coulomb failure model are determined (Lechner et al., 2021). For this a three-point bending experiment and a compression test are needed. The mechanical experiments are performed on a Z020 universal testing machine (ZwickRoell GmbH & Co. KG, Ulm, Germany) with a 20 kN force sensor. The bending experiment is performed with 150 mm distance between the supports on the bending beam described above. The compression test is performed with a cube, which is acquired by shortening the bending beam to 20 mm. A 1 mm polymer sheet is put between the core material and the testing machine on both contact surfaces to achieve a continuous and smooth stress field in the cube. Without this sheet, the pressure of the testing machine is not induced equally into the cube, due to the rough and brittle surface of the specimen. The bending and the compression test setup are shown in Fig. 2.

2.3. Material modelling

Inorganic core materials exhibit a brittle failure behaviour and therefore follow the weakest-link theory and are best described with Weibullian failure statistics, as shown by Lechner et al. (2018). They further showed in a previous article, that IOB core materials follow a weakest-link based Mohr–Coulomb model (Lechner et al., 2021):

$$\begin{aligned} exp[\ & -\left(\frac{0.5|\sigma_1 - \sigma_2|}{0.5(\sigma_1 + \sigma_2)\cdot sin(-\phi) + c\cdot cos(-\phi)}\right)^m \\ & -\left(\frac{0.5|\sigma_2 - \sigma_3|}{0.5(\sigma_2 + \sigma_3)\cdot sin(-\phi) + c\cdot cos(-\phi)}\right)^m \\ & -\left(\frac{0.5|\sigma_3 - \sigma_1|}{0.5(\sigma_3 + \sigma_1)\cdot sin(-\phi) + c\cdot cos(-\phi)}\right)^m] \\ = \ & exp1^{-1}, \end{aligned} \tag{2}$$

where σ_{1-3} are the principle stresses. c and ϕ are the Mohr–Coulomb parameters. This criterion assumes a shear stress induced failure, as common Mohr-Coulomb models. Classic Mohr–Coulomb criteria

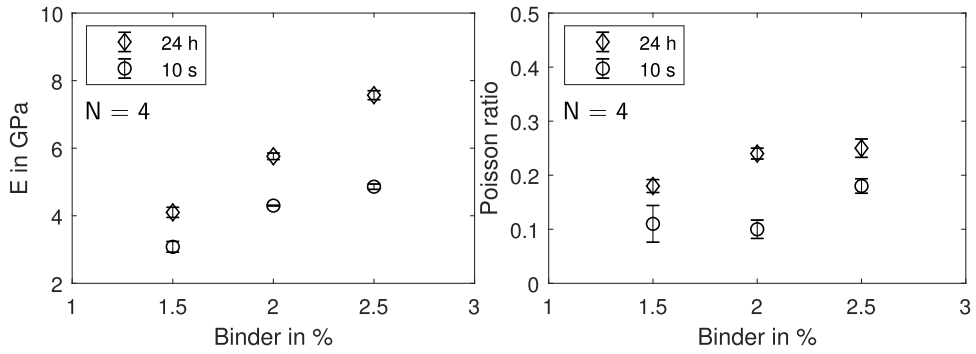

Fig. 4. Young's Modulus E and Poisson ratio for IOB core materials directly after the core shooting and after 24 h for varying amounts of binder. The error intervals show the minimal and maximal values in the data set.

consider only the highest principal shear stress. In contrast, Eq. (2) takes the failure probability of all three principal shear stress into account.

According to Weibull's theory, the effective volumes of the specimens have to be considered to compare two different specimens and load cases. For ceramics, the effective volume is calculated with respect to the maximum local principle stress and the maximum global principle stress. This reasoning is based on the assumption that ceramics follow a principle stress yield criterion. According to Gong (2003), the usual equation to calculate the effective volume for uni-axial stress states is:

$$V_{\text{eff}} = \int_V \left(\frac{\sigma}{\sigma_{\max}}\right)^m \mathrm{dV}, \tag{3}$$

where σ is the local stress in the volume cell used for the integration, m is the Weibull shape parameter and σ_{max} is the maximum principal stress in the specimen at the point of failure. However, the Mohr–Coulomb model utilised in this article (Lechner et al., 2021) is based on the shear stress hypothesis. Therefore the effective stress in the core should be calculated based on all three principle shear stress components.

$$V_{\text{eff}} = \sum_{i=1}^{3} \int_V \left(\frac{\tau_i}{\tau_{\max}}\right)^m \mathrm{dV}, \tag{4}$$

$$\tau_1 = \frac{|\sigma_1 - \sigma_2|}{2}, \tag{5}$$

$$\tau_2 = \frac{|\sigma_2 - \sigma_3|}{2}, \tag{6}$$

$$\tau_3 = \frac{|\sigma_3 - \sigma_1|}{2}, \tag{7}$$

where τ_i are the shear stresses calculated from principle stresses σ_i in the volume element and τ_{max} is the biggest shear stress in the whole component. Comparing specimens with a shape factor m and different volumes V, the failure stress σ_s follows:

$$\frac{V_1}{V_2} = \left(\frac{\sigma_{s_2}}{\sigma_{s_1}}\right)^m. \tag{8}$$

2.4. Validation test

In order to validate the described material model, a complex water jacket core was utilised. This water jacket core is subjected to various load cases on the universal testing machine. Fig. 3 shows these load cases on the left side. The water jacket core is placed on a stiff plate and subjected vertically with an increasing force at three different points of contact by the testing machine. The load points are indicated by the red arrows. The load is increased until the specimen breaks and the maximum force is considered the failure force.

2.5. Finite element simulation

A finite-element simulation model was built in Abaqus (Dassault Systems, Velizy-Villacoublay, France) to calculate the complex stress states analogously to the experiments described in the section before. The goal is to predict the yield force of the water jacket core for each load case. The model is meshed with approximately 1.3 million tetrahedral C3D10M elements which are well suited for the hard contact between the support and the core. Furthermore, they were chosen for their advantages in meshing complex parts. In areas with increased stresses, the mesh is refined to 0.3 mm seed distance to achieve a more precise result, while the mesh in the rest of the core is kept at 3.5mm seed distance to improve the numerical performance. A detailed view of the mesh in the regions of interest is shown on the right side of Fig. 3. The boundary conditions are as follows: The water jacket core is placed upon a plate, which is defined as an analytic rigid. The contact is defined as friction-less in tangential direction and a hard contact in normal direction. All degrees of freedom of the analytical rigid plate are fixed. The loads are chosen as surface pressure in the area, which was subjected to the load in the real experiment and increased linearly. A dynamic explicit solver without time or mass scaling was utilised.

In order to evaluate the effective volume for the increasing load force, the principal stresses and the volume of each element is exported every 5 N. These data sets are imported into Matlab and evaluated for the effective volume with Eq. (4).

The failure force is determined by evaluating the exported data with Eq. (2). The first frame, which violates this failure surface, is utilised to determine the failure force.

3. Results and discussion

In the following, the material parameters immediately after the core shooting and after 24 h of storage are determined. These values describe the lower and upper limits of the material parameters which have to be considered for core handling simulations, since core materials typically continue to harden in storage. The immediate material parameters were determined 10 s after the opening of the tool. Since it was not possible to manufacture the cubic compression test specimen from the beam in 10 s, experiments 120 s after tool opening were added, where necessary.

3.1. Elastic parameters

In a first step, the elastic parameters for three amounts of binder and for two points in time after the core shooting (10 s and 24 h) were determined. The results are shown in Fig. 4. To quantify the scatter in the data, the interval from the minimal to the maximal value is depicted for each data point, while the number of specimens is indicated with N. In general, the Young's modulus and the Poisson ratio are increasing with the binder amount. For both parameters, the values are higher after

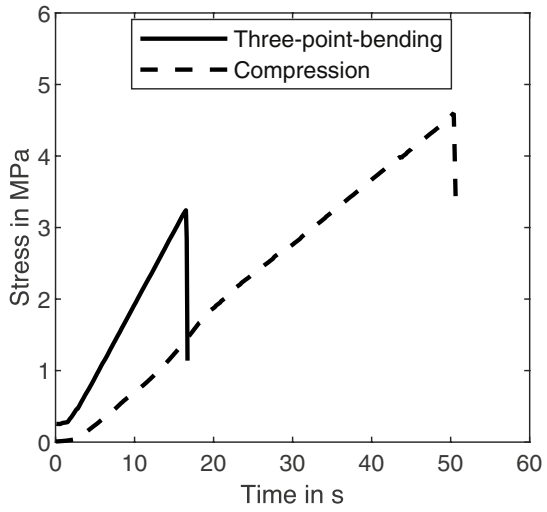

Fig. 5. Examples of stress-time curves, which are determined with the bending and the compression test setup.

24 h of storage than after 10 s. This shows, that the condensation reaction, which solidifies the sand-binder compound continues after the removal from the core box. The 24h-Young's modulus E_{24h} is increasing approximately linear, while the 10 s-Young's modulus E_{10s} starts to saturate for 2.5% liquid binder. Schneider et al. (2018) predicted this near-linear increase of E_{24h} with micro-structure simulations, which could not be confirmed at the time. It seems intuitive that the Young's modulus is increasing with the amount of binder, since the sand-binder compound should become stiffer with more binder. However, the Poisson ratio is increasing as well, which translates to a higher transversal contraction. With the assumption of isotropic material behaviour, this implies that the Young's modulus is increasing more than the shear modulus according to Eq. (1). The material stiffness, which influences the elongation and compression behaviour of the material and correlates to the Young's modulus, is predominantly determined by the number and size of the binder bridges in the sand binder micro-structure. In contrast, the shear stiffness is influenced to a higher degree by the size and form of the grains and less by the binder bridges themselves. Therefore, there is a stronger correlation of the Young's modulus to the amount of binder compared to the shear modulus.

3.2. Mohr–Coulomb characterisation

In order to parametrise the failure criterion described with Eq. (2), the bending and compression strength of the IOB materials was determined. The strength data points are determined for different conditions typical for the life cycle of the cores:

- Immediately after the core shooting (10 s and 120 s), which is also called the "immediate strength".
- After a longer storage period (24 h), which is called "storage strength"
- After a 24 h storage period with an additional heat treatment at 450 °C for 30 min, which emulates a casting process, which is called "decoring strength".

Typical examples of the unfiltered stress-time data determined with the test setups are shown in Fig. 5. Both data sets show signs of brittle fracture. The strength data is shown in Fig. 6. Please note, that the immediate compressive strength 10s after the core shooting was not determined, since it was not possible to shorten the beam-shaped specimen to the cubic sample in the time available. An approximately linear correlation between the binder amount and the tensile and compressive strength 10 s and 24 h after tool opening can be detected.

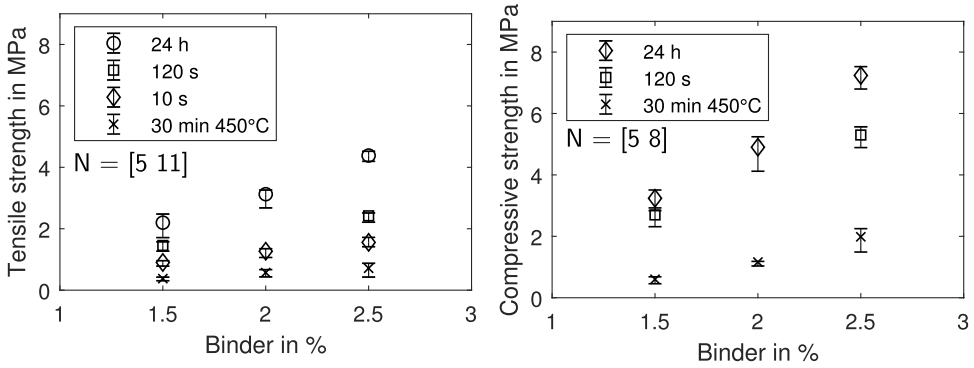

Fig. 6. Tensile and compressive strength data for various storage conditions and binder amounts. The error intervals show the minimal and maximal values in the data set.

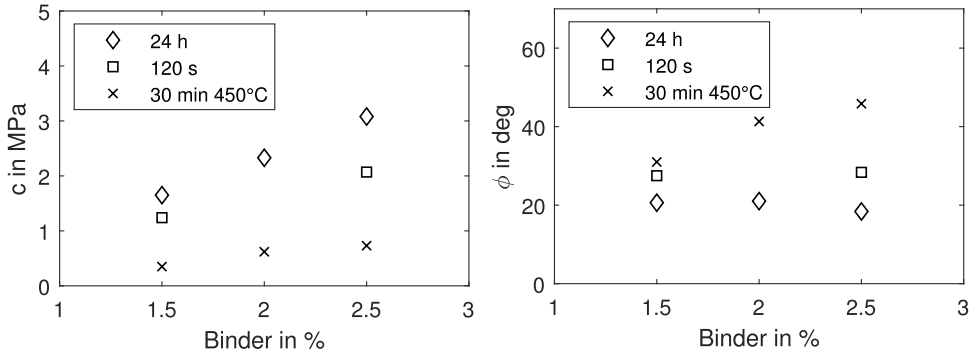

Fig. 7. Mohr–Coulomb parameters c and ϕ for various storage conditions and binder amounts.

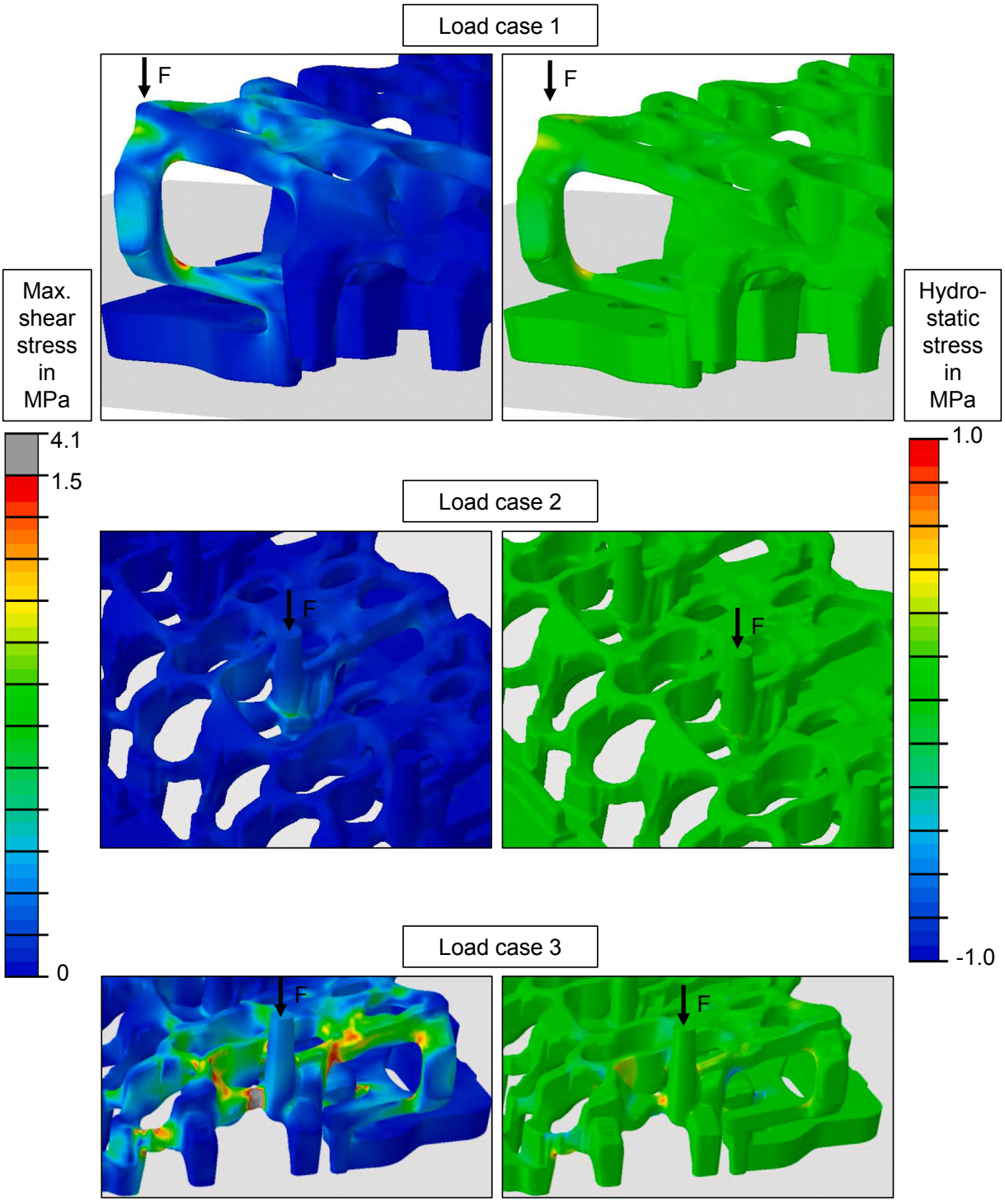

Fig. 8. FEM results of the water jacket core for all load cases at 10 N load. On the left side the maximum shear stresses are depicted, on the right side the hydrostatic pressure. Both are important influences on the Mohr–Coulomb failure criterion.

Furthermore, the 30 min heat treatment of the specimens does not change the linear correlation of the strength values. Only two binder amounts are available 120 s after tool opening, but based on the other data points a linear correlation can be assumed as well. Similar to the Young's modulus, the storage strength is higher than the immediate strength after the core shooting. The strength of the specimens with heat treatment is strongly decreased compared to the specimens without heat treatment. The tensile strength falls below the immediate strength after 10 s.

After scaling the test results to the same effective volume with Eqs. (4) and (8), the tensile and compressive test results can be introduced as uni-axial stress states in Eq. (2) to solve for c and ϕ via least-square error minimisation. From the strength data an average Weibull shape factor m for Eq. (2) can be calculated. The results for c and ϕ are shown in Fig. 7 for the effective volume of the 3-point-bending experiment. It is not surprising that c is increasing linearly with the binder amount, since it is mainly determined by the absolute values of the tensile and compression strength. ϕ is mainly determined by the ratio of the tensile and compressive strength, independent of their absolute values. The closer the tensile strength σ_t is to the compressive strength σ_c, the smaller the

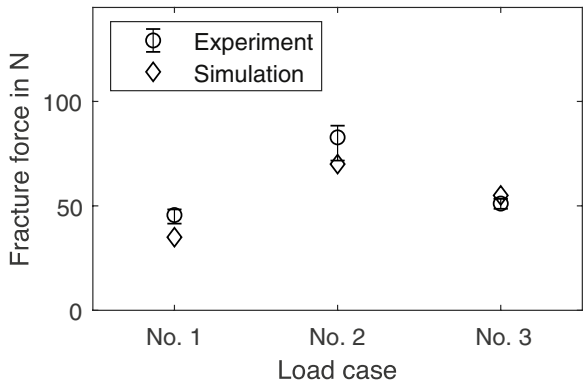

Fig. 9. failure forces of the water jacket core for various load cases. The experimental results are marked with circles, while the simulation results are indicated by diamond symbols.

friction angle becomes. The extreme value would be $\phi = 0$ for $\sigma_t = \sigma_c$. ϕ is approximately constant for all conditions. The friction angle of the specimens with heat treatment ϕ_{HT} is higher than ϕ_{24h} at room temperature. This shows that the weakening effect of the heat treatment is decreasing the tensile strength more than the compressive strength, which leads to a higher friction angle. Furthermore, the friction angle ϕ_{120s} is higher than ϕ_{24h}. The binder is still hardening, which is increasing the tensile strength more than the compressive strength and thus lowering ϕ.

3.3. *Prediction of core failure for a water jacket core*

The material model was validated with water jacket cores, which were produced with 2% liquid binder. These water jacket cores were subjected to three loadcases as described in Section 2.4. Please note that due to the quantity and dimensions of the water jacket cores, they could not be stored in a climate chamber as the other test specimens. They were stored at usual room conditions. To ensure that the material parameters from Section 3.2 are still accurate, some test specimens were stored with the water jacket cores and compared their strength results to those of the specimens from the climate chamber. They were approximately equal.

Simultaneously, the loads were simulated with FEM and increased the load in 5 N steps. The result is shown in Fig. 8 for a load of 10 N. The stress data is exported to Matlab and evaluated for a failure according to Eq. (2). The effective volume at the failure load is determined and the material parameters are scaled with weibullian statistics to this effective volume. The results of the experiments and the simulations are shown in Fig. 9. There is a good agreement between the simulation and the experiments, when considering a brittle material, which is very sensitive to stress concentrations. Fig. 10 shows an exemplary fractured specimen for the load cases one and three and compares them to the stress peaks in the simulation. The fracture locations coincide well with the position of the stress peaks. Load case two fractured the specimens into multiple parts, which makes it difficult to analyse the fracture origin. The results show that the material model is suitable to dimension the binder amount in the water jacket core according to specific handling load cases.

4. Industrial application

In modern casting processes, the binder amount of foundry cores is chosen with respect to the estimated necessary strength of the cores and the necessary hot strength during the casting. In this decision process, the handling strength defines the absolute minimum amount of necessary binder, while depending on the casting process, more binder might be necessary to achieve a stable process with high quality products.

At the moment, handling stresses are only estimated based on previous successful components. This leads to a potential to save binder by a true dimensioning process in FEM with a digital twin of the handling processes from the core shooting machine to the casting mould. This has economical and ecological benefits since it directly saves binder during the core shooting. But it also saves energy and time during the de-coring at the end of the casting process, since lower binder amounts lead to a lower remaining core strength, as shown by the experiments. Izdebska-Szanda et al. (2012) stated that for inorganically-bound core materials, the remaining core strength after the casting is one of the biggest draw backs compared to organic binder systems. However, by reducing the binder amount for parts with enough hot strength, the de-coring

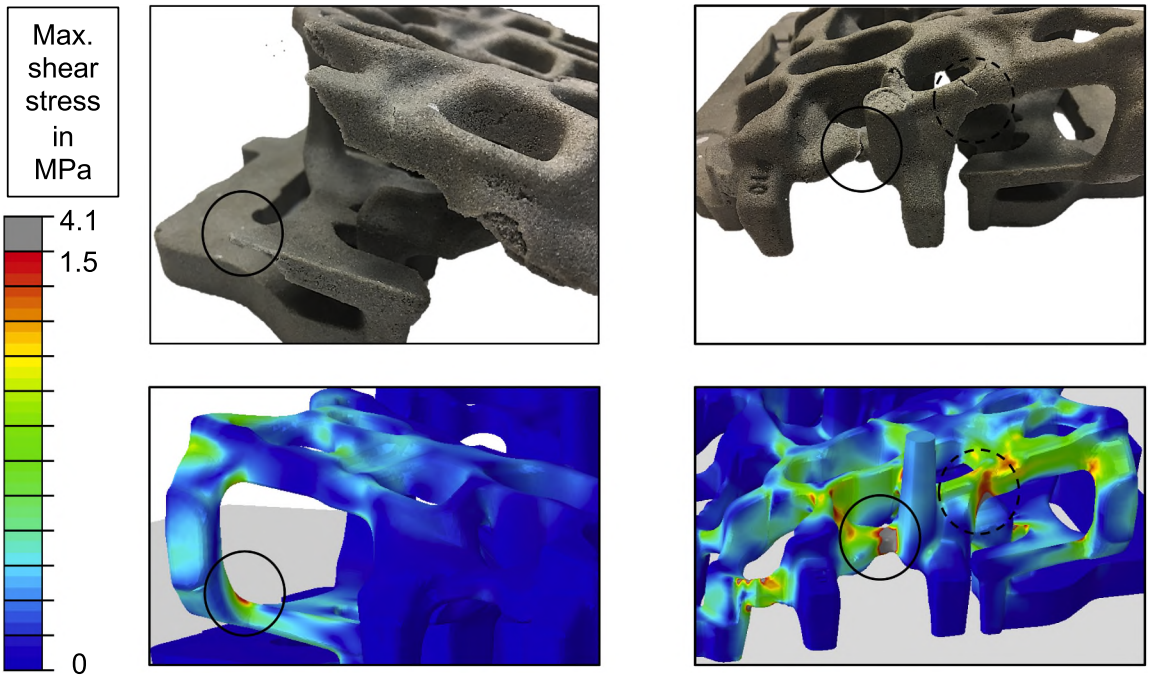

Fig. 10. Fracture locations of load case one and three (top) compared to the stress peaks in the simulation (bottom).

problem might be improved considerably without additional investment in higher impact energy de-coring technology. After a simulation of the handling processes, the minimal strength is known and can be utilised to calculate the necessary binder amount by a simple regression with a few support points and varying binder amounts. This was shown with the variation of the Inotec binder (1.5%, 2.0%, 2.5%) as an example. For each process step which has to be simulated, a material characterisation has to be performed to know the momentary Mohr-Coulomb parameters, since the immediate strength is considerably lower than the 24 h strength. Alternatively, the worst case calculation based on the immediate strength can be performed for all handling processes.

Furthermore, the data from the specimens with heat treatment indicate that core materials follow the same type of yield model, with a higher friction angle ϕ after the casting. This is a first step to actually calculating the stresses which are induced into the cores during the de-coring processes, which can help to optimise them. Galles and Beckermann (2015) proposed that due to the volume contraction of the cast component, the cores are under hydrostatical pressure after the casting. This explains, together with the fact that cores follow a Mohr–Coulomb yield criterion, why the de-coring process is more difficult, than the significantly reduced bending strength after heat treatment indicates. The bending experiment is performed at significantly lower hydrostatical pressure than the de-coring of the cast parts.

5. Conclusion

In this article, a material model was utilised, which was previously published by Lechner et al. (2021) for inorganically-bound core materials. This model was generalised for various conditions in the life-cycle of the core. It was implemented into a FEM simulation and validated by predicting core failures for complex geometries and stress states. Now a consistent and validated material model is available to simulate typical production processes like core handling and storage. With this model the minimal binder amount can be calculated, which is necessary to bring the core from the core shooting machine to the mould without damage. This optimisation brings technical and economic benefits, since reduced binder amounts save resources directly, but also reduces the de-coring effort after the casting indirectly.

Declaration of Competing Interest

The authors report no declarations of interest.

Acknowledgements

This research was supported by DFG grant No. 401764392. We would like to thank Loramendi S. Coop., Aurenak S. Coop.L., Quarzwerke GmbH and ASK Chemicals GmbH for providing the materials and tools needed for conducting this research. We are grateful to BMW AG for providing the water jacket geometry for research purposes. Furthermore, we would like to thank Benjamin Himmel for providing valuable feedback to this article.

References

Banganayi, F.C., Nyembwe, D.K., Polzin, H., 2020. Optimisation of an environmentally friendly foundry inorganic binder core making process for the replacement of an organic binder. MRS Adv. 5 (25), 1323–1330.

Bargaoui, H., Azzouz, F., Thibault, D., Cailletaud, G., 2017. Thermomechanical behavior of resin bonded foundry sand cores during casting. J. Mater. Process. Technol. 246, 30–41.

Bührig-Polaczek, A., Träger, H., 2010. Foundry technology. In: Ullmann's encyclopedia of industrial chemistry. Vol. 1. Wiley, Chichester, p. 271.

Caylak, I., Mahnken, R., 2010. Thermomechanical characterisation of cold box sand including optical measurements. Int. J. Cast Met. Res. 23 (3), 176–184.

Dong, S., Iwata, Y., Hohjo, H., Iwahori, H., Yamashita, T., Hirano, H., 2010. Shell mold cracking and its prediction during casting of ac4c aluminum alloy. Mater. Trans. 51 (8), 1420–1427.

EN 843-2, 2006. Advanced technical ceramics - mechanical properties of monolithic ceramics at room temperature - part 2: Determination of young's modulus, shear modulus and poisson's ratio.

Fan, Z.T., Huang, N.Y., Dong, X.P., 2004. In house reuse and reclamation of used foundry sands with sodium silicate binder. Int. J. Cast Met. Res. 17 (1), 51–56.

Galles, D., Beckermann, C., 2015. Effect of sand dilation on core expansion during steel casting. IOP Conference Series: Materials Science and Engineering 84, 012022.

Gong, J., 2003. Correlation between weibull moduli for tensile and bending strength of brittle ceramics: a numerical simulation analysis based on a three-parameter weibull distribution. J. Mater. Sci. 38.

Granat, K., Nowak, D., Pigiel, M., Stachowicz, M., Wikiera, R., 2008. The influence of water glass on the properties of microwave cured molding sands. Archiv. Foundry Eng. 8.

Holtzer, M., Kmita, A., 2020. Sodium silicate molding sands. In: Holtzer, M., Kmita, A. (Eds.), Mold and Core Sands in Metalcasting: Chemistry and Ecology. Vol. 18. Springer International Publishing, Cham, pp. 219–241.

Izdebska-Szanda, I., Angrecki, M., Matuszewski, S., 2012. Investigation of the knocking out properties of moulding sands with new inorganic binders used for casting of non-ferrous metal alloys in comparison with the previously used. Archiv. Foundry Eng. 12.

Kammerer, D., Essbauer, S., 2009. World's first emission-free foundry: Bmw group's light-alloy foundry goes over to new ecofriendly sand core production. Press Release - BMW AG, p. 2009.

Lechner, P., Fuchs, G., Hartmann, C., Steinlehner, F., Ettemeyer, F., Volk, W., 2020. Acoustical and optical determination of mechanical properties of inorganically-bound foundry core materials. Materials 13 (11). URL https://www.mdpi.com/1996-1944/13/11/2531.

Lechner, P., Hartmann, C., Ettemeyer, F., Volk, W., 2021. A plane stress failure criterion for inorganically-bound core materials. Materials (Basel, Switzerland) 14 (2).

Lechner, P., Stahl, J., Ettemeyer, F., Himmel, B., Tananau-Blumenschein, B., Volk, W., 2018. Fracture statistics for inorganically-bound core materials. Materials 11 (11). URL https://www.mdpi.com/1996-1944/11/11/2306.

Pabel, T., Kneissl, C., Schumacher, P., Brotzki, J., Müller, J., 2012. 10 Improved properties of aluminium cast parts through the use of inorganic cores. Foundry Trade J. Int. 196, 257–261.

Polzin, H., 2014. Inorganic binders: for mould and core production in the foundry. Fachverlag Schiele & Schön.

Schneider, M., Hofmann, T., Andrä, H., Lechner, P., Ettemeyer, F., Volk, W., Steeb, H., 2018. Modelling the microstructure and computing effective elastic properties of sand core materials. Int. J. Solids Struc. 143, 1–17.

Stachowicz, M., Granat, K., Nowak, D., 2011. Influence of water-glass grade and quantity on residual strength of microwave-hardened moulding sands. part 2. Archiv. Foundry Eng. 11 (2), 143–148.

Stachowicz, M., Palyga, L., Kepowicz, D., 2020. Influence of automatic core shooting parameters in hot-box technology on the strength of sodium silicate olivine moulding sands. Archiv. Foundry Eng. 67–72.

Stauder, B.J., Berbic, M., Schumacher, P., 2019. Mohr-coulomb failure criterion from unidirectional mechanical testing of sand cores after thermal exposure. J. Mater. Process. Technol. 274, 116274.

Stauder, B.J., Harmuth, H., Schumacher, P., 2018. feb De-agglomeration rate of silicate bonded sand cores during core removal. J. Mater. Process. Technol. 252, 652–658.

Stauder, B.J., Kerber, H., Schumacher, P., 2016. nov Foundry sand core property assessment by 3-point bending test evaluation. J. Mater. Process. Technol. 237, 188–196.

Thorborg, J., Kumar, S., Wagner, I., Sturm, J.C., 2020. The virtual core - modelling and optimization of core manufacturing and application. IOP Conference Series: Materials Science and Engineering 861, 012004.

Vasková, I., Varga, L., Prass, I., Dargai, V., Conev, M., Hrubovčáková, M., Bartošová, M., Bulko, B., Demeter, P., 2020. Examination of behavior from selected foundry sands with alkali silicate-based inorganic binders. Metals 10 (2), 235.

Xin, F.-h., Liu, W.-h., Song, L., Li, Y.-m., 2020. Modification of inorganic binder used for sand core-making in foundry practice. China Foundry 17 (5), 341–346.